Reprinted from December 1987, Vol. 109, Journal of Applied Mechanics

Identification of Nonlinear Vibrating Structures: Part II—Applications

S. F. Masri

R. K. Miller

A. F. Saud

Department of Civil Engineering,
University of Southern California,
Los Angeles, CA 90089-0242

T. K. Caughey

Division of Engineering and Applied Science,
California Institute of Technology,
Pasadena, CA 91106

A time-domain procedure for the identification of nonlinear vibrating structures, presented in a companion paper, is applied to a "calibration" problem which incorporates realistic test situations and nonlinear structural characteristics widely encountered in the applied mechanics field. The "data" set is analyzed to develop suitable, approximate nonlinear system representations. Subsequently, a "validation" test is conducted to demonstrate the range of validity of the method under discussion. It is shown that the procedure furnishes a convenient means for constructing reduced-order nonlinear nonparametric mathematical models of reasonably high fidelity in regard to reproducing the response of the test article under dynamic loads that differ from the identification test loads.

1 Introduction

1.1 Background. In the study by Masri et al. (1987b), henceforth referred to as the "companion paper," the authors presented the formulation of a time-domain method for the identification of arbitrarily nonlinear multi-degree-of-freedom (MDOF) vibrating systems undergoing free vibrations or subjected to direct force excitations and/or support motion that is not necessarily uniform. This paper applies the identification procedure in the cited reference to a "calibration" problem which incorporates realistic test situations and nonlinear characteristics. Subsequently, a "validation" problem is considered to invesitgate the range of validity of the identification/prediction procedure.

1.2 Scope. Section 2 of this paper defines the model configuration, the nonlinear (polynomial and hysteretic) element characteristics, and the exact system parameters corresponding to the "small oscillations" range.

Section 3 discusses a synthetic "experiment" meant to simulate a conventional "hammer-blow" test that is routinely used in contemporary experimental modal analysis procedures. After describing the probing signal characteristics and input/output measurements, the data processing approach under consideration is used to extract the linearized system inertia, damping and stiffness matrices.

Section 4 is concerned with a simulated forced vibration test wherein the excitation (stationary, wide-band random) is not directly applied to the system but rather to its moving support points. By using the parametric identification results for the linearized system parameters obtained in Section 3, the time histories of the nonlinear forces involving all system degrees of freedom are obtained. Using the eigenvectors associated with the linearized system as basis functions to transform the "measured" nonlinear forces, the generalized nonlinear forces and corresponding generalized state variables are obtained. Applying the nonparametric identification procedure under discussion, and approximating analytical function involving a series expansion in terms of a set of orthogonal polynomials is obtained and shown to yield a good estimate of the presumably unknown nonlinear restoring forces of the system.

Section 5 is concerned with the "validation" of the present identification procedure by using the identification results obtained in Section 4 to predict (estimate) the response of the "exact" nonlinear system, when the location of the disturbance as well as its form is different from what was used for the probing signal in the identification phase discussed in Section 4.

2 Model Characteristics

2.1 Example System Characteristics. To illustrate the application of the method under discussion, consider the hypothetical finite element model shown in Fig. 1. This one-dimensional (rectilinear horizontal motion) structure consists of three nearly equal masses m_i, $i=1,2,3$ that are interconnected by means of six truss elements anchored to an interface at three locations, thus resulting in a redundant system with three degrees of freedom.

The absolute displacement of each m_i is designated by x_i, while the prescribed motion of the three support points are designated by $s_i(t)$, $i=1,2,3$. The three excitation forces that directly act on the system components are denoted by $F_i(t)$, $i=1,2,3$. Thus, in terms of the notation introduced in the companion paper,

Contributed by the Applied Mechanics Division for publication in the JOURNAL OF APPLIED MECHANICS.

Discussion on this paper should be addressed to the Editorial Department, ASME, United Engineering Center, 345 East 47th Street, New York, N.Y. 10017, and will be accepted until two months after final publication of the paper itself in the JOURNAL OF APPLIED MECHANICS. Manuscript received by ASME Applied Mechanics Division, January 13, 1987; final revision June 23, 1987.

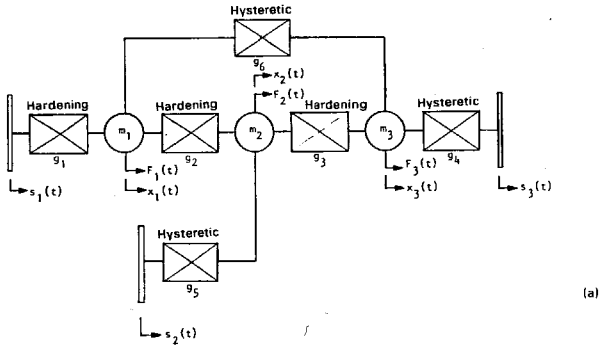

$m_1 = 0.8, \quad m_2 = 2.0, \quad m_3 = 1.2$

Element (i)	Type	$p_1^{(i)}$	$p_2^{(i)}$	$p_3^{(i)}$	$p_4^{(i)}$	$p_5^{(i)}$
1	Hardening	2.0	0.2	1.0		
2	Hardening	1.0	0.1	20.0		
3	Hardening	1.0	0.1	20.0		
4	Hysteretic	2.0	0.2	1.0	0.0	0.4
5	Hysteretic	2.0	0.2	1.0	0.0	0.4
6	Hysteretic	1.0	0.1	0.5	0.0	0.4

(b)

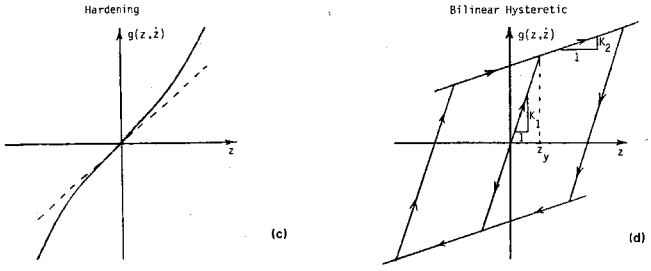

Fig. 1 Model of example nonlinear 3DOF system: (a) configuration; (b) element characteristics; (c) generic element with polynomial nonlinearity; (d) generic element with bilinear hysteretic properties. $x_i(t)$ designates the absolute displacement of m_i, and $s_j(t)$ designates the absolute displacement time history associated with the support DOF$_j$.

(a)

$$M = \begin{pmatrix} 0.8 & 0.0 & 0.0 \\ 0.0 & 2.0 & 0.0 \\ 0.0 & 0.0 & 1.2 \end{pmatrix} \quad C = \begin{pmatrix} 0.4 & -0.1 & -0.1 \\ -0.1 & 0.4 & -0.1 \\ -0.1 & -0.1 & 0.4 \end{pmatrix} \quad K = \begin{pmatrix} 4.0 & -1.0 & -1.0 \\ -1.0 & 4.0 & -1.0 \\ -1.0 & -1.0 & 4.0 \end{pmatrix}$$

(b)

$$\phi = \begin{pmatrix} 1.000 & 1.000 & 1.000 \\ 1.735 & -1.242 & -0.093 \\ 1.165 & 2.511 & -0.342 \end{pmatrix} \quad \omega = \begin{pmatrix} 1.173 \\ 1.848 \\ 2.354 \end{pmatrix} \quad \zeta = \begin{pmatrix} 0.0587 \\ 0.0924 \\ 0.1177 \end{pmatrix}$$

Fig. 2 (a) Exact values of linearized system matrices corresponding to the small oscillations (infinitesimal) motion range. (b) Modal characteristics involving the matrices *M*, *C*, and *K* corresponding to fixed-base motion.

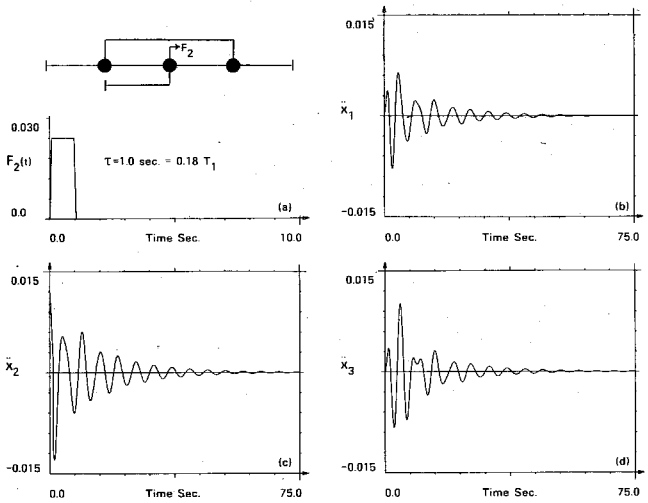

Fig. 3 Acceleration time history of the three masses in the nonlinear system under "hammer-blow" test applied to mass m_2. The duration of the impulsive excitation is approximately 0.18 of the system's fundamental period. (a) F(t); (b) $\ddot{x}_1(t)$; (c) $\ddot{x}_2(t)$; (d) $\ddot{x}_3(t)$. The same amplitude and time scale is used for all plots. Time span shown covers approximately 14 fundamental periods.

$$\mathbf{x}_1(t) = (x_1, x_2, x_3)^T, \tag{1}$$

$$\mathbf{x}_0(t) = (s_1, s_2, s_3)^T, \tag{2}$$

$$\mathbf{f}_1(t) = (F_1, F_2, F_3)^T, \tag{3}$$

$n_1 = 3$ and $n_0 = 3$.

The arbitrary nonlinear elements, denoted by g_i, that are interposed between the masses and between the support points are dependent on the relative displacement z and the velocity $\dot{z}$ across the terminals of each element. In the case of polynomial nonlinearities, the elements assume that form,

$$g_i(z, \dot{z}) = p_1^{(i)} z + p_2^{(i)} \dot{z} + p_3^{(i)} z^3, \tag{4}$$

where $p_1^{(i)}$ is the linear stiffness component, $p_2^{(i)}$ is the linear viscous damping term, and $p_3^{(i)}$ corresponds to the coefficient of the nonlinear (cubic) displacement term. Thus, depending on the sign of $p_3^{(i)}$, the form of g_i in equation (4) can be made to represent restoring forces with hardening or softening nonlinearities—a commonly encounterd type of nonlinearity in physical systems.

The form of the nonlinearity expressed by equation (4) is a polynomial-type without cross-product terms. To illustrate the wide applicability of the present method, a hysteretic-type restoring force will be considered. Such a nonlinearity not only involves cross-product terms of displacement and velocity, but is of course not even expressible in polynomial form. Hysteretic systems, widely encountered in all areas of applied mechanics (e.g., building and equipment systems, as well as aerospace structures containing collapsible or retractable elements), are among the more difficult types of nonlinear properties to investigate and identify (Caughey, 1960, 1975; Iwan, 1965, 1966; Iwan and Lutes, 1968; Jennings, 1964; Lutes and Takemiya, 1974; Andronikou and Bekey, 1984).

In the example structure under discussion, three elements (g_1, g_2, and g_3) have hardening-type polynomial nonlinear properties, and the remaining three elements (g_4, g_5, and g_6) have bilinear hysteretic properties characterized by the following parameters:

$p_1^{(i)} = k_1$ = stiffness in the elastic range,
$p_2^{(i)} = c_1$ = viscous damping term in the linear range,
$p_3^{(i)} = k_2$ = stiffness in the nonlinear range,
$p_4^{(i)} = c_2$ = viscous damping term in the nonlinear range,
$p_5^{(i)} = z_y$ = yield displacement level.

The magnitudes of the system masses as well as the material properties of the nonlinear model elements are tabulated in Fig. 1(*b*).

Notice that the structure of the model is not chain-like, consequently the linearized system stiffness matrix is not banded. The exact values of the system mass, damping, and stiffness matrices corresponding the an infintesimal ("small oscillations") range of the motion in the neighborhood of the position of static equilibrium are shown in Fig. 2 together with the associated mode shapes, natural frequencies, and modal damping values corresponding to a fixed-base configuration of the model.

$$M = \begin{pmatrix} 0.804 & 0.000 & 0.000 \\ 0.000 & 2.000 & 0.000 \\ 0.000 & 0.000 & 1.203 \end{pmatrix} \quad C = \begin{pmatrix} 0.403 & -0.100 & -0.102 \\ -0.100 & 0.400 & -0.100 \\ -0.102 & -0.100 & 0.401 \end{pmatrix} \quad K = \begin{pmatrix} 4.03 & -1.00 & -1.01 \\ -1.00 & 4.00 & -1.00 \\ -1.01 & -1.00 & 4.01 \end{pmatrix}$$

$$\phi = \begin{pmatrix} 1.000 & 1.000 & 1.000 \\ 1.734 & -1.242 & -0.093 \\ 1.164 & 2.512 & -0.341 \end{pmatrix} \quad \omega = \begin{pmatrix} 1.173 \\ 1.848 \\ 2.355 \end{pmatrix} \quad \zeta = \begin{pmatrix} 0.0586 \\ 0.0923 \\ 0.1177 \end{pmatrix}$$

$$\frac{\omega - \omega^{(i)}}{\omega^{(i)}} = \begin{pmatrix} 0.00\ \% \\ 0.00\ \% \\ 0.04\ \% \end{pmatrix} \quad \frac{\zeta - \zeta^{(i)}}{\zeta^{(i)}} = \begin{pmatrix} -0.17\ \% \\ -0.11\ \% \\ 0.00\ \% \end{pmatrix}$$

Fig. 4 Parametric identification under impulsive direct force excitation. Formulation is for a full-order system with symmetric matrices under forced vibrations. Time segment used for identification is about two fundamental periods.

3 Impulsive Excitations and Response Measurement

3.1 Probing Signal. The method under consideration imposes no restrictions on the nature of the excitation source to be used as a probing signal. It will be assumed in the present example that an impulsive excitation (resembling a "hammer blow" disturbance of the type widely used in modal analysis techniques) is applied to mass m_2.

When the above-mentioned excitation is applied to the example structure, segments of the resulting acceleration time histories of the three mass locations would be as shown in Fig. 3. The same scale is used for all locations to make relative magnitude comparison easier. The time duration shown corresponds to about 15 system fundamental periods T_1.

3.2 Data Processing. By integrating the measured acceleration time histories shown in Fig. 3, the time histories of the corresponding velocities and displacments are obtained. From that, inter-element deformations $z_i(t)$ and velocities $\dot{z}_i(t)$ can be determined.

3.3 Parametric Identification. In what follows, the task of identifying the system matrices (determining the linearized system influence coefficients) will be referred to as the "parametric" identification phase of the procedure. Conversely, the task of developing an approximating analytical representation for the nonlinear forces involved in the system motion will be referred to as the "nonparametric" identification phase of the current procedure. For convenience, a prefix *A* will henceforth be used to indicate that a referenced section, equation, or figure is in the companion paper mentioned above.

With reference to the notation introduced earlier in the companion paper, the general parametric identification procedure can be applied to the present case by noting that the problem is one in which the number of degrees of freedom is $n_1 = 3$, the number of support degrees of freedom is $n_0 = 0$ (i.e., no support motion), and the number of nonzero excitation force components is $n_f = 1$ (since only $F_2(t) \neq 0$)

By using the recursive weighted least-squares approach discussed in Section *A*2.2, the symmetric system matrices M_{11}, C_{11}, and K_{11} are identified and shown in Fig. 4. Comparing the elements of matrices M_{11}, C_{11}, and K_{11} shown in Figs. 2 and 4 shows that, if all the response measures are used to identify the dynamic system, then the identified results are accurate to within a few percent for all system parameters, insofar as the infintesimal range of motion is concerned. The small discrepancies are attributable to slight changes in the nonlinear elements. Further details regarding the application of the parametric identification procedure, under a variety of test situations, are available in the work by Masri et al. (1987a).

4 Random Base Excitation Test

4.1 Probing Signals and Response. The motion of the

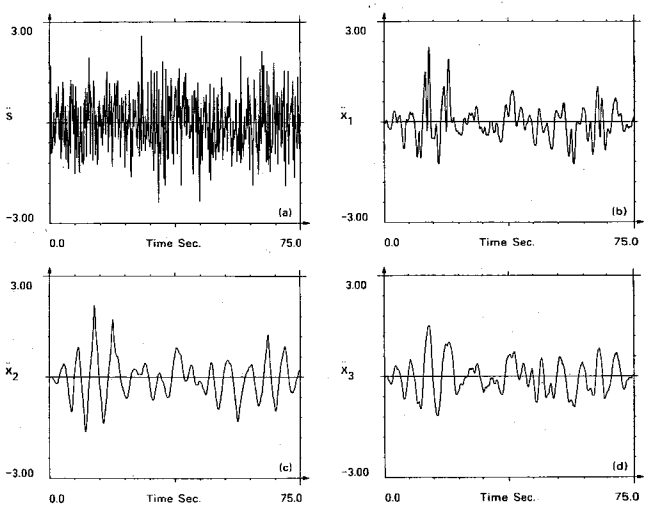

Fig. 5 Acceleration time history of the base motion $\ddot{s}(t)$ and the response $\ddot{x}_i(t)$ of the three masses in the nonlinear system shown in Fig. 1 under uniform base excitation applied to the three supports. Identical amplitude and time scales are used for all the plots. Time segment shown corresponds to approximately 14 fundamental periods of the linearized system. Input is stationary, wide-band random excitation with a flat power-spectral-density.

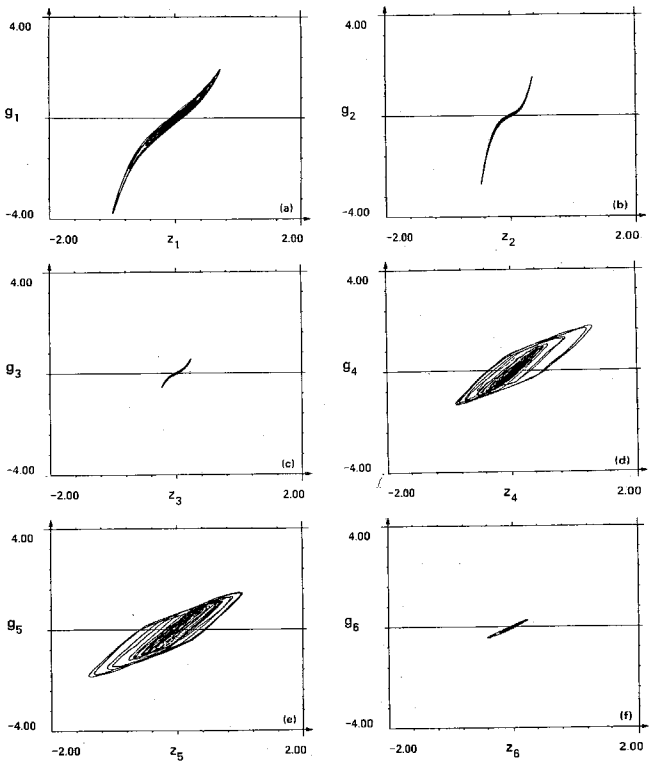

Fig. 6 Phase-plane plots of the six elements in the form of force-deformation characteristics g_i and z_i involving the nonlinear system finite elements when subjected to the uniform stationary random base excitation shown in Fig. 5

stucture discussed in Section 3 consisted of essentially small oscillations. In the present "test," the structure is assumed to be subjected to uniform, wide-band random support accelerations $\ddot{s}_1(t)$, $\ddot{s}_2(t)$, and $\ddot{s}_3(t)$. This particular choice of excitation is intended to mimic a situation in which a structure with multiple load paths is subjected to a random support motion of the type furnished by shaking tables.

4.2 Data Processing. For more realistic simulation, it will be further assumed that the only available

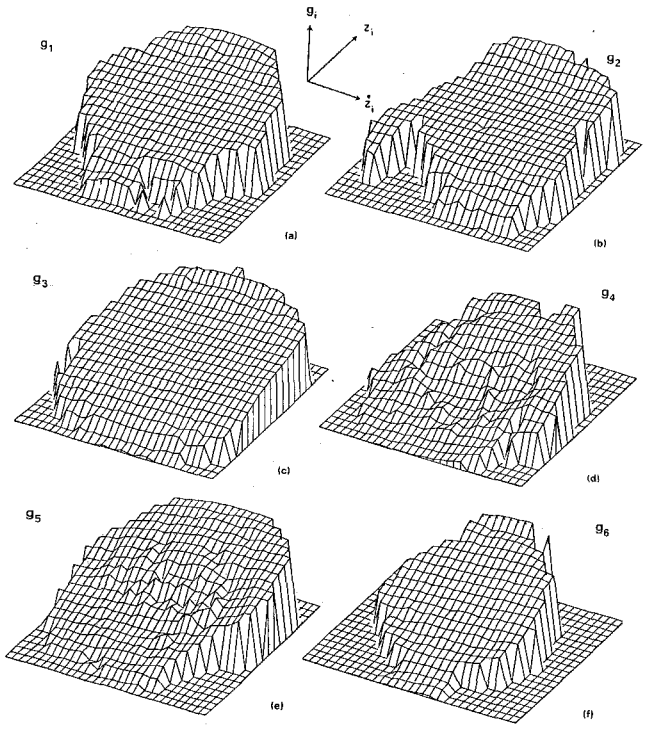

Fig. 7 Three-dimensional representation of the force deformation characteristics of the six finite elements of the system when subjected to wide-band random base acceleration

"measurements" are those of the acceleration of the three supports, $(\ddot{s}_i(t),\ i=1,2,3)$, and the acceleration of the three masses $(\ddot{x}_i(t),\ i=1,2,3)$: None of the system velocities or displacements are directly measured. A representative segment of each of the excitations (chosen, for simplicity, to be the same) and responses is shown in Fig. 5. To facilitate comparisons, the same amplitude scale is used for like response quantites at different locations. By processing the measured accelerations, the system velocities and displacements are obtained.

Phase-plane plots of all the elements' force-deformation curves are shown in Fig. 6. Unlike the results obtained under impulsive excitation, it is clear from the inspection of Fig. 6 that elements g_1, g_2, and g_3 have a hardening-spring characteristic, while elements g_4 and g_5 are undergoing hysteretic behavior. A three-dimensional representation of the resistance characteristics of each of the elements is shown in Fig. 7.

4.3 Parametric Identification Procedure. In the most general case for the example under discussion, the parametric identification procedure can be used to determine the elements of the six matrices M_{11}, C_{11}, and K_{11}, each of order $n_1 \times n_1$, and matrices M_{10}, C_{10}, and K_{10}, each of order $n_1 \times n_0$, where $n_1=3$ and $n_0=3$ and $n_f=0$ (since no direct excitation is applied). However, to further demonstrate the flexibility of the present method, the previously determined system matrices in Section 3, based on the "small oscillations" response, will be used as is (i.e., not recomputed). Thus, the remaining system matrices to be identified are M_{10}, C_{10}, and K_{10}. Furthermore, for simplicity, it will be assumed that the system mass matrix is diagonal. This implies that M_{10} is a null matrix.

With the above assumptions in mind, the parametric identification procedure can be expressed as:

$$C_{10}^{(e)}\dot{\mathbf{x}}_0 + K_{10}^{(e)}\mathbf{x}_0 = -(M_{11}^{(i)}\ddot{\mathbf{x}}_1 + C_{11}^{(i)}\dot{\mathbf{x}}_1 + K_{11}^{(i)}\mathbf{x}_1). \tag{5}$$

The superscripts (i) and (e) attached to the definition of the system matrices appearing above designate "infinitesimal-motion range" and "equivalent linear," respectively.

Notice that, in the present case, the number of independent support motions is equal to unity since the motion of the three support points is uniform. Consequently, $n_1=3$, $n_0=1$, $n_f=0$, $\eta_{\alpha 1}=2n_0=2$, and the total number of unknown

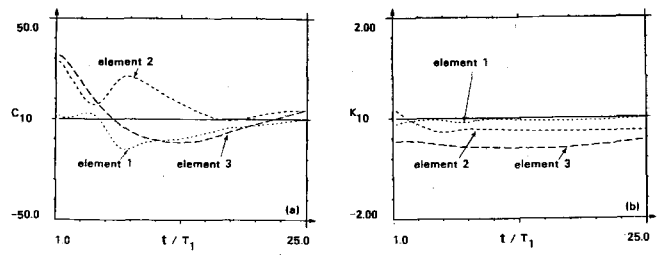

$$C_{10} = \begin{pmatrix} -0.196 \\ -0.183 \\ -0.176 \end{pmatrix} \qquad K_{10} = \begin{pmatrix} -2.00 \\ -2.00 \\ -2.00 \end{pmatrix}$$

Fig. 8 The evolution of the element values of the identified matrices as a percentage of the exact value of the corresponding "infinitesimal motion range"

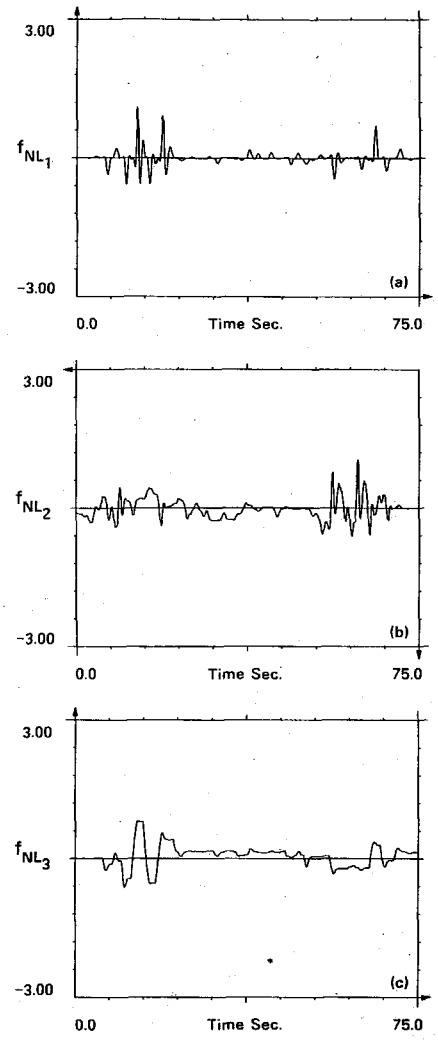

Fig. 9 Time history of the three components of the nonlinear residual force vector $f_N(t)$ obtained from the equation of motion by subtracting the contribution of the identified linear inertia, damping, and stiffness forces. The same amplitude and time scale is used for all plots. The amplitude scale matches the corresponding scale used in Fig. 5 to plot the time history of the system accelerations. The time scale used covers approximately 14 fundamental periods T_1.

Notice that, in the present case, the number of independent support motions is equal to unity since the motion of the three support points is uniform. Consequently, $n_1=3$, $n_0=1$, $n_f=0$, $\eta_{\alpha 1}=2n_0=2$, and the total number of unknown

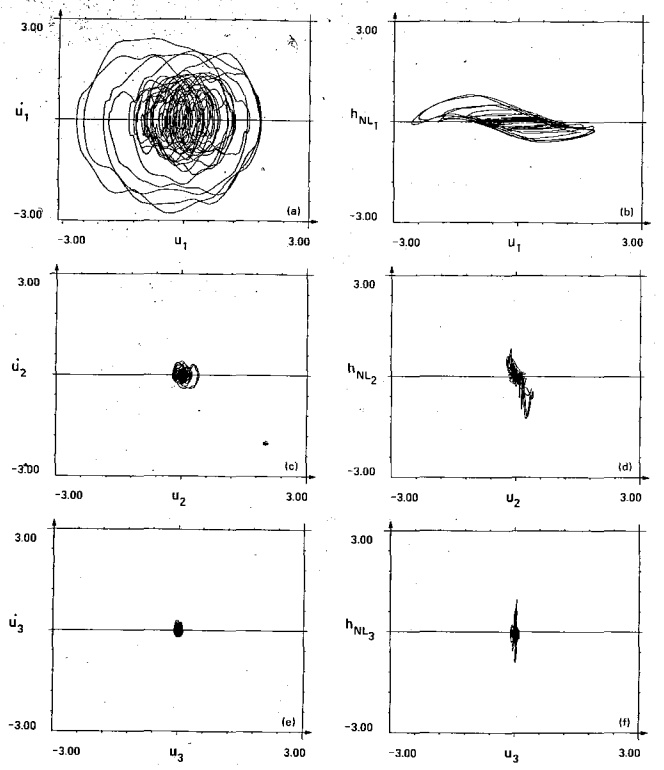

Fig. 10 Phase-plane plots of the "modal" state variables u_i and $\dot{u}_i$ and the three generalized nonlinear residual forces h_i with respect to the corresponding generalized displacement u_i. Identical horizontal and vertical scales are used for all plots. Note from plot (*b*) the clear evidence of the hysteretic behavior involved with the first mode.

parameters to be identified at this stage is $\eta_\alpha = n_1 \eta_{\alpha 1} = 6$. The results of the procedure are shown in Fig. 8.

The evolution of the magnitude of the identified system matrices $C_{10}^{(e)}$ and $K_{10}^{(e)}$ with time, obtained through the recursive algorithm discussed in the companion paper, is also shown in Fig. 8. For convenience, the magnitude of the ordinate of the plotted parameters have been normalized by the "exact" value of the corresponding "infinitesimal-motion range" parameters. The abscissa of the curves appearing in Fig. 8 have been normalized by T_1, the system fundamental period in the "small oscillations" range. Consequently, the ordinate of Fig. 8(*a*) covers a range ±50 percent relative to the unity value of the ratio $c_{0_j}^* = (c_{0_j}^{(e)}/c_{0_j}^{(i)})$, $j = 1,2,3$ where $c_{0_j}^{(e)}$ and $c_{0_j}^{(i)}$ is the single element in row j of the column matrix $C_{10}^{(e)}$ and $c_{10}^{(i)}$, respectively. Similarly, the ordinate of Fig. 8(*b*) covers a range ±2.0 percent relative to the unity value of the ratio $k_{0_j}^* = (k_{0_j}^{(e)}/k_{0_j}^{(i)})$, $j = 1,2,3$ where $k_{0_j}^{(e)}$ and $k_{0_j}^{(i)}$, is the element in row j of column matrix $K_{10}^{(e)}$ and $K_{10}^{(i)}$, respectively. The abscissa of the plots in both parts (*a*) and (*b*) in Fig. 8 covers a range of about $25T_1$.

It is worth noting from Fig. 8 that the spread of the results (i.e., dimensionless ordinate scales of the two plots) pertaining to the damping and stiffness influence coefficients differ by more than an order of magnitude (a factor of about 50). This behavior is consistent with the fact that, in the example under discussion, the relative contribution of damping-related forces and stiffenss-related forces is nearly inversely proportional to the above-mentioned spread.

4.4 Determination of Nonlinear Forces. Using the available measurements and the previously identified system matrices, the nonlinear system forces can now be computed from

$$\mathbf{f}_N(t) = \mathbf{f}_1(t) - (M_{11}^{(i)}\ddot{\mathbf{x}}_1 + C_{11}^{(i)}\dot{\mathbf{x}}_1 + K_{11}^{(i)}\mathbf{x}_1 + C_{10}^{(e)}\dot{\mathbf{x}}_0 + K_{10}^{(e)}\mathbf{x}_0 \tag{6}$$

(a) h_1 coefficients

$v_1 = u_1$ $\quad v_{1_{min}} = -2.5801$ $\quad v_{1_{max}} = 1.8444$

$v_2 = \dot{u}_1$ $\quad v_{2_{min}} = -2.7806$ $\quad v_{2_{max}} = 2.4147$

	$T_0(v_2)$	$T_1(v_2)$	$T_2(v_2)$	$T_3(v_2)$	$T_4(v_2)$	$T_5(v_2)$
$T_0(v_1)$	0.0430	0.4553	0.0978	0.0808	0.0330	-0.0071
$T_1(v_1)$	-0.1634	-0.0093	0.0245	0.0097	0.0786	0.0101
$T_2(v_1)$	-0.0577	0.0274	0.0351	-0.0199	-0.0050	-0.0118
$T_3(v_1)$	0.0736	-0.0003	0.0037	-0.0023	-0.1118	-0.0098
$T_4(v_1)$	0.0074	0.0228	0.0176	-0.0215	-0.0141	-0.0271
$T_5(v_1)$	-0.0081	0.0204	-0.0414	-0.0038	0.0171	-0.0120

(b) h_2 coefficients

$v_1 = u_2$ $\quad v_{1_{min}} = -0.2250$ $\quad v_{1_{max}} = 0.4094$

$v_2 = \dot{u}_2$ $\quad v_{2_{min}} = -0.4007$ $\quad v_{2_{max}} = 0.4080$

	$T_0(v_2)$	$T_1(v_2)$	$T_2(v_2)$	$T_3(v_2)$	$T_4(v_2)$	$T_5(v_2)$
$T_0(v_1)$	-0.1024	0.1227	-0.0011	0.1102	0.0190	0.0120
$T_1(v_1)$	-0.4054	-0.0229	0.0339	0.0295	0.0832	0.0622
$T_2(v_1)$	0.0154	0.0162	0.0007	-0.0254	-0.0292	-0.0083
$T_3(v_1)$	-0.0398	0.0564	-0.0105	-0.1108	-0.0794	-0.0304
$T_4(v_1)$	0.0837	0.0335	0.0296	-0.0705	-0.0621	-0.0084
$T_5(v_1)$	-0.0389	-0.0057	-0.0429	0.0415	-0.0387	0.0017

(c) h_3 coefficients

$v_1 = u_3$ $\quad v_{1_{min}} = -0.1047$ $\quad v_{1_{max}} = 0.1100$

$v_2 = \dot{u}_3$ $\quad v_{2_{min}} = -0.2076$ $\quad v_{2_{max}} = 0.3060$

	$T_0(v_2)$	$T_1(v_2)$	$T_2(v_2)$	$T_3(v_2)$	$T_4(v_2)$	$T_5(v_2)$
$T_0(v_1)$	-0.0180	-0.0912	0.0805	0.0009	0.0609	-0.0351
$T_1(v_1)$	-0.0331	0.0361	-0.0117	-0.0406	0.0298	0.0158
$T_2(v_1)$	-0.0139	-0.0314	0.0492	-0.0105	0.0287	-0.0288
$T_3(v_1)$	-0.0267	-0.0201	0.0104	-0.0145	0.0009	0.0119
$T_4(v_1)$	-0.0071	0.0200	-0.0121	0.0048	-0.0146	0.0133
$T_5(v_1)$	0.0066	-0.0193	-0.0237	0.0474	-0.0047	0.0210

Fig. 11 Nonparametric identification results. Note that the indicated coefficients correspond to the normalized Chebyshev polynomials.

With that, the time history of the nonlinear force vector $\mathbf{f}_N(t)$ components can be determined and are shown in Fig. 9. For convenience, identical scales are used for the three plots.

At this stage of the identification procedure, the "best" (in least-squares sense) equivalent linear model has been determined in the form of the identified matrices. Thus, if for the purposes of a particular application the norm of the residual error, $\|\mathbf{f}_N(t)\|$, as computed from equation (6) is sufficiently small, then the identification task can be terminated. For more demanding situations, additional processing is required to more accurately identify the residual forces that have been determined.

As pointed out earlier, if there is a need to augment the parametric identification results with additional results from the nonparametric phase of the data processing, one can proceed directly to develop approximating analytical representations, for as many of the components of $\mathbf{f}_N(t)$ as warranted, in terms of a series expansion involving suitable generalized coordinates. However, when the order of the dynamic system is relatively large, dealing with a transformed set of nonlinear forces may lead to a faster rate of convergence of the applicable series.

A convenient and natural transformation to use with realistic dynamic systems is the one expressed by equation (*A*33):

$$\mathbf{h}(\mathbf{u}, \dot{\mathbf{u}}) = \Phi^T \mathbf{f}_N(t), \tag{7}$$

$$\mathbf{u}(t) = \Phi^{-1}\mathbf{y}_1(t), \tag{8}$$

where

$$y_{1_j} = x_{1_j} - x_{0_j} \qquad j = 1,2,3, \tag{9}$$

and Φ is the modal matrix associated with $M_{11}^{-1}K_{11}$. Although the linear modal transformation of equation (8) does *not* lead

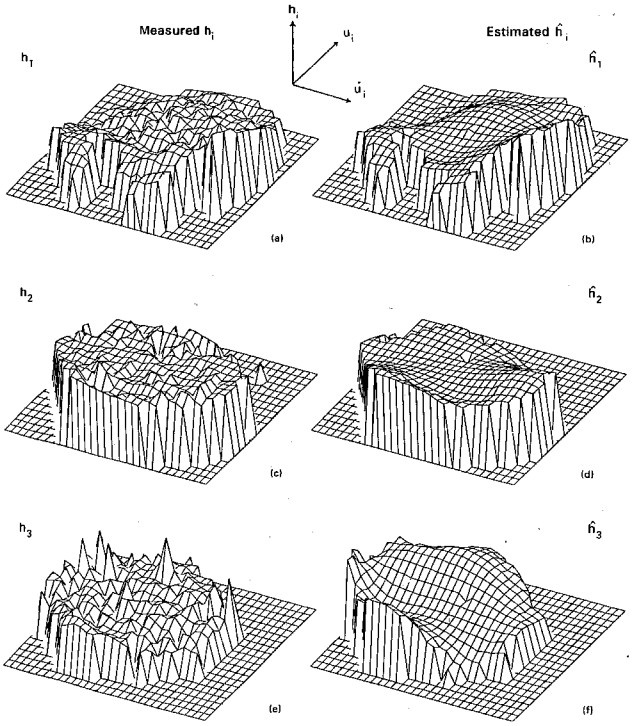

Fig. 12 (a), (c), and (e): Three-dimensional representation of the variation of each of the three generalized nonlinear forces h_i with the corresponding state variables u_i and $\dot{u}_i$; (b), (d), and (f): three-dimensional plots of the estimated (identified) generalized nonlinear forces $\hat{h}_i$ as a function of the corresponding state variables. For better resolution, different scales are used for each of the three plots.

to a decoupled set of equations in this nonlinear case, it has been found in many examples to lead to an increased rate of convergence of the series representation of the nonlinear force vector $\mathbf{f}_N(t)$. The time history of the "modal" state variables $\mathbf{u}(t)$ and $\dot{\mathbf{u}}(t)$ as well as the "modal" nonlinear forces computed in accordance with the above equations, are shown in the form of phase plots in Fig. 10.

The plots of the estimated modal restoring forces versus their corresponding modal displacement in Fig. 10 clearly indicate the presence of hysteretic components in the system.

4.5 Nonparametric Identification Procedure. Using Chebyshev polynomials in accordance with equation (*A*41) to obtain two-dimensional fits for the surfaces of the modal restoring functions will yield the typical identification results tabulated in Fig. 11. Three-dimensional representation of the transformed nonlinear forces in terms of their corresponding state variables are shown in Fig. 12 together with the approximating functions $\hat{h}_{N_j}$, $j=1,2,3$.

It is clear from the Tables of Fig. 11 that determining the optimum least-squares fit for the data associated with the hysteretic system does involve many cross-product terms in displacement and velocity. It also requires a relatively larger number of terms in the series (six used in the present example) for a good estimate.

The preceding is a good illustration of the need to use two-dimensional surface fits rather than the uncoupled one-dimensional series to estimate the system properties. Whether cross-coupling is significant or not is a decision that need not be made a priori when following the method presented here—the system will effectively "decide" by its own response (signature) the extent and relative dominance or contribution arising from various powers of $T_i(u)T_j(\dot{u})$.

Examination of the projections of h_i on u_j indicates negligible modal coupling in the present example. Such may not be the case in other applications. However, the presented method

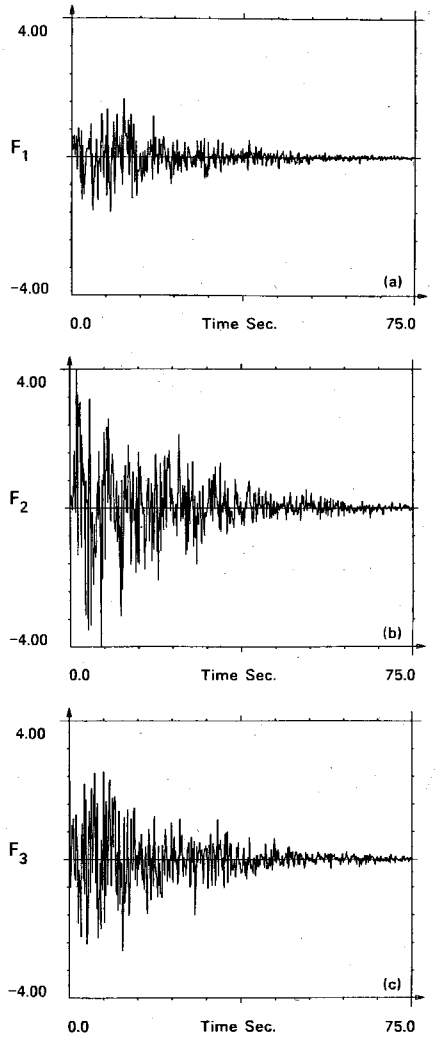

Fig. 13 Nonstationary excitation used in the validation test

can cope with nonlinear modal coupling by simply adding as many cross-coupling terms as necessary (see equation (*A*41)).

5 Response Prediction Under Different Excitation

In order to demonstrate the validity of the present identification approach, the model representation expressed by the C_{kl} coefficients shown in Fig. 11, which were extracted from the original ("exact") modal response under a probing signal consisting of stationary broad-band excitation, supplied through support motion, will now be used to predict the response of the original model when subjected to directly-applied (to mass m_2) nonstationary random excitation consisting of modulated white noise of the form

$$p_o(t) = e(t)n(t), \tag{10}$$

where $e(t)$ is a deterministic envelope function

$$e(t) = a_1 e^{a_2 t} + a_3 e^{a_4 t}, \tag{11}$$

with the a's being deterministic constants, and $n(t)$ is the output of a simulated Gaussian white noise process. The excitation time histories are shown in Fig. 13.

By following the steps indicated in equation (*A*15), the identification results can be used to predict the response time history. The adequacy of the approximate (identified) nonlinear model to predict the response of the exact (hysteretic) nonlinear system under arbitrary excitation is clearly illustrated by the results shown in Fig. 14 in which the "exact" relative displacement of each mass location of the

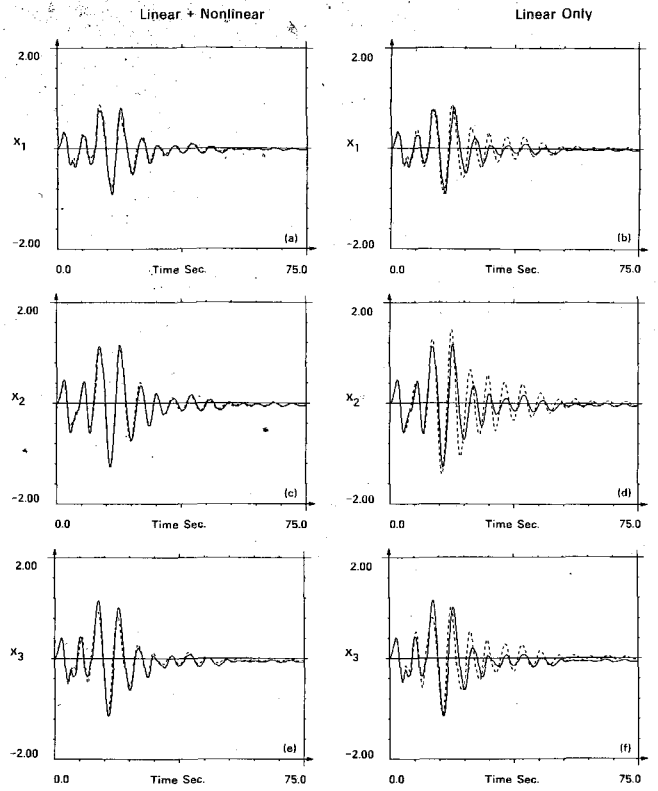

Fig. 14 Comparison between the measured and predicted response time history (*a*), (*c*), and (*e*) when both the linear and nonlinear terms are used; (*b*), (*d*) and (*f*) when only linear terms are used

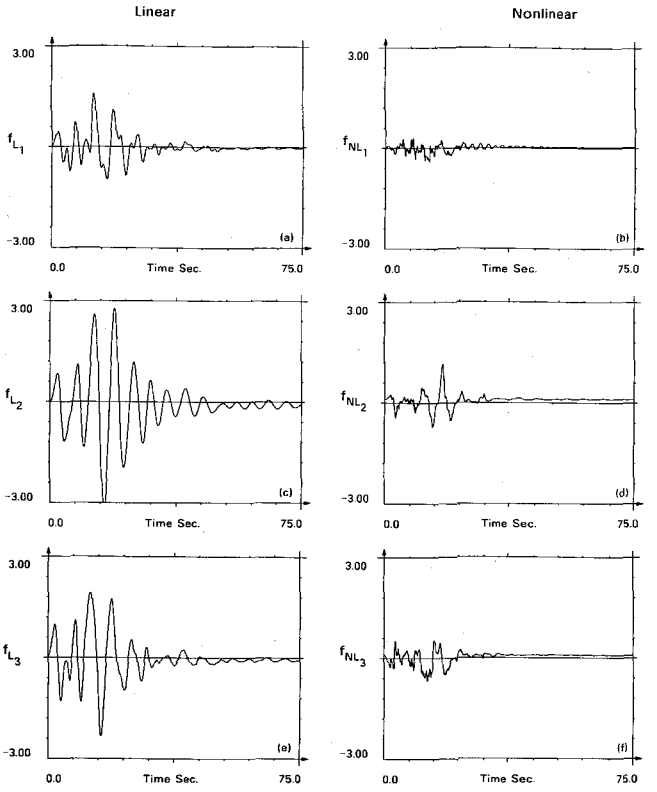

Fig. 15 Comparison between the contribution of the linear and nonlinear terms of the internal forces associated with the system degrees of freedom

nonlinear system is compared to its corresponding value as computed on the basis of the approximate nonlinear model.

The plots on the right-hand-side column of Fig. 14 show a comparison between the time history of the measured and predicted elements' deformation when only linear terms are used to compute the estimated response. Note that the exclusion of the nonlinear terms from the indentification results leads to a deterioration in the accuracy (of the amplitude as well as the phase) of the predicted response. The contribution of the nonlinear terms to the internal forces associated with the system degrees of freedom is compared to the corresponding linear terms in Fig. 15. Note that, as one would expect, the magnitude of these forces is correlated with the large amplitude range of motion.

6 Summary and Conclusions

Application of a time-domain procedure for the identification of nonlinear vibrating structures, presented in a companion paper, to a multi-degree-of-freedom nonlinear system incorporating hysteretic and polynomial-type nonlinearities, demonstrates the utility of the method under discussion. It is shown that an optimum (in the least-squares sense) reduced-order nonlinear mathematical model can be developed to match, with reasonable accuracy, all of the response time histories measured by the available sensors. Furthermore, the mathematical representation allows convenient separation of the contribution of the linear and nonlinear internal forces developed in the structure.

The illustrative examples indicate the considerable flexibility inherent in the procedure to cope with a variety of data processing and test performance situations.

Acknowledgment

This study was supported in part by a grant from the National Science Foundation and the National Institute of Health Biomedical Simulations Resource at the University of Southern California.

References

Andronikou, A. M., and Becky, G. A., 1979, "Identification of Hysteretic Systems," *Proc. of the 18th IEEE Conf. on Decision and Control*, Dec., pp. 1072–1073.

Caughey, T. K., 1960, "Random Excitation of a System with Bilinear Hysteresis," ASME JOURNAL OF APPLIED MECHANICS, Vol. 27, No. 4, Dec., pp. 649–652.

Caughey, T. K., 1975, "Nonlinear Analysis, Synthesis and Identification Theory," *Proc. Symposium on Testing and Identification of Nonlinear Systems*, California Institute of Technology, Mar., pp. 1–14.

Distefano, N., and Todeschini, R., 1974, "Modeling, Identification and Prediction of a Class of Nonlinear Viscoelastic Materials," *International Journal of Solids and Structures*, Part I, Vol. 9, pp. 805–818.

Hudson, D. E., "Equivalent Viscous Friction for Hysteretic Systems with Earthquake-Like Excitation," *Proc. 3WCEE*, New Zealand.

Iwan, W. D., 1965, "The Steady-State Response of the Double Bilinear Hysteretic System," ASME JOURNAL OF APPLIED MECHANICS, Vol. 32, No. 4, Dec., pp. 921–925.

Iwan, W. D., 1966, "A Distributed-Element Model for Hysteresis and Its Steady-State Dynamic Response," ASME JOURNAL OF APPLIED MECHANICS, Vol. 33, No. 4, Dec., pp. 893–900.

Iwan, W. D., and Lutes, L. D., 1968, "Response of the Bilinear Hysteretic System to Stationary Random Excitation," *Journal of the Acoustical Society of America*, Vol. 43, No. 3, Mar., pp. 545–552.

Jennings, P. C., 1964, "Periodic Response of a General Yielding Structure," *ASCE Journal of Engineering Mechanics Division*, Vol. 90, No. EM2, pp. 131–166.

Jennings, P. C., 1968, "Equivalent Viscous Damping for Yielding Structures," ASCE *Journal of Engineering Mechanics*, Feb.

Lutes, L. D., and Takemiya, H., 1974, "Random Vibration Damping of Yielding Oscillator," *ASCE Journal of the Engineering Mechanics Division*, Vol. 100, No. EM2, pp. 343–358.

Masri, S. F., Miller, R. K., Saud, A. F., and Caughey, T. K., 1987, "Identification of Nonlinear Vibrating Structures," University of Southern California Report No. USC-CE 8710, June.

Masri, S. F., Miller, R. K., Saud, A. F., and Caughey, T. K., 1987, "Identification of Nonlinear Vibrating Structures; Part I: Formulation," ASME JOURNAL OF APPLIED MECHANICS, Vol. 54, No. 4, Dec.